Supporting Information

Achieving Bright Organic Light Emitting Field Effect Transistors with Sustained Efficiency through Hybrid Contact Design

*Shih-Wei Chiu[1], An Hsu[1], Lei Ying[2], Yong-Kang Liaw[1], Kun-Ta Lin[1], Jrjeng Ruan[1], Ifor D. W. Samuel[3] and Ben B. Y. Hsu[1]**

1 *Department of Materials Science and Engineering, National Cheng Kung University, Taiwan.*

2 *Institute of Polymer Optoelectronic Materials and Devices, State Key Laboratory of Luminescent Materials and Devices, South China University of Technology, Guangzhou 510640, P. R. China.*

3 Organic Semiconductor Centre, SUPA, School of Physics and Astronomy, University of St Andrews, U.K.

Table of Content:

*Corresponding author: hsubon@gmail.com

S1. The particle analysis, transmittance, electroluminescence, and reliability test on the hybrid drains:

In order to study the correlation between optical scattering and different morphology on the hybrid drains, we analyze the particle diameter distribution of Figure 2a by the software (ImageJ). The results are shown in Figure S1 (left) without Au and (right) with Au. Without Au, larger Ag particles with their average diameter r=9.9 nm indeed increased optical scattering and the film looked bluish. These particles show strong Rayleigh scattering effect $2\pi r/\lambda \ll 1$; λ and r are scattering wavelength and particle diameter. Larger Ag clusters produced blues color as Rayleigh scattering describes, which is a drawback for a light emitting device. Oppositely, 1 nm Au produced a smooth Ag layer composed of finer Ag particles with r=3.9 and the film looked transparent which could be seen through. The transmission spectra and the insets of Figure S2a show that the improved wettability of Au:Ag on SPFN can produce clear and transparent metal contacts. In Figure S2b, the transparent hybrid drain can successfully emit the EL of SY like Figure S2b that matches not only the commonly found spectra but the highest transmission wavelength range in Figure S2a. Overall scattering of light is suppressed by the smooth surface and small particles.

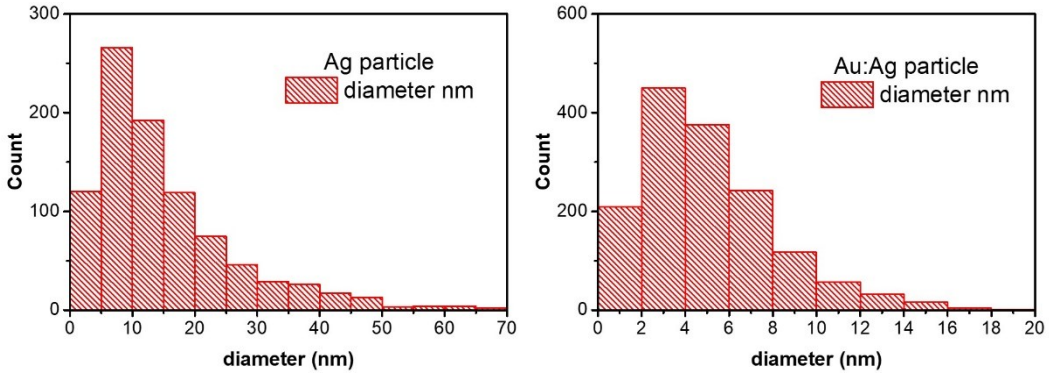

Figure S1 The diameter distributions of Ag particles without (left) and with (right) the 1 nm Au wetting layer.

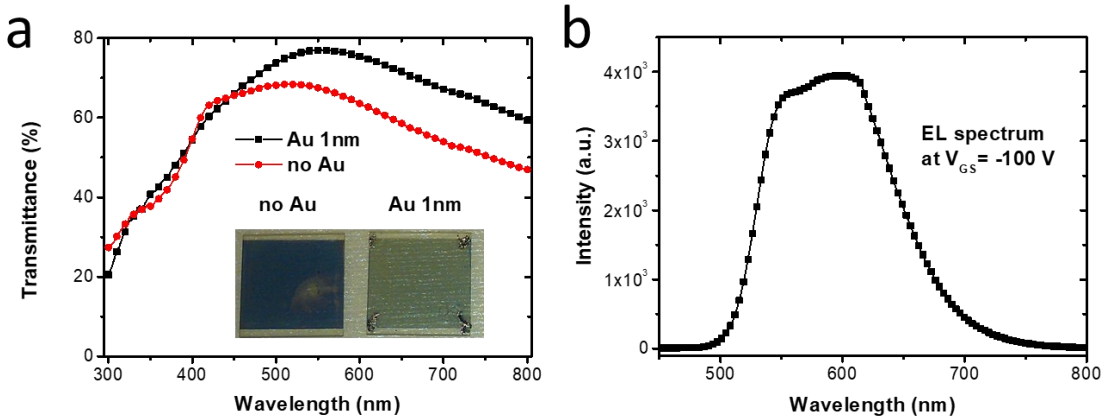

Figure S2 (a) The transmission spectra of the hybrid drain with and without 1 nm Au on SPFN polyelectrolyte. The inset shows the two hybrid contacts grown on glass substrates. (b) The EL spectrum of an HC-OLEFET operated at V_{GS}=V_{DS}= -100 V.

Using high-molecular weight (high-Mw) SPFN with fabric-like topography, we found that the roughness of SPFN layer dominates the transmittance of the hybrid drain when the MoO_x thickness< 40 nm, as shown in Figure S3. When 40 nm> MoO_x thickness >20 nm, the maximum transmittance regimes of MoO_x on both SPFN show similar profiles and values. However, fabric-like morphology with roughness R_q=3.1 nm (Figure S3a) blue-shifts the maximum transmittance about 80% from 550−630 nm to 350−450 nm and decreases the transmittance with increasing MoO_x thickness. On the other hand, low-M_n SPFN was found to increase transmittance with the increasing MoO_x thickness and reach its maximum at 20 to 30 nm MoO_x (See Figure S2, S3e, and S3f). The opposite tendencies of transmittance varied with MoO_x thicknesses indicate that SPFN dominates photon extraction. To maximize transmittance, we suggest low-M_n SPFN which can be smoothened by the solvent-flushing treatment.

MoO_x may vary the transparency more significantly at larger thickness. However, due to the need for sufficient conductivity, the MoO_x thickness should be less than 30 nm and low-M_n SPFN is recommended for high performance. Otherwise, the resistive drain will seriously degrade the performance. As seen in Figure S4, OLED composed of PATBT/SY/SPFN/Au:Ag/MoO_x like HC-OLEFETs demonstrates a functional diode I-V curve with reliable ON/OFF. However, electrical conduction is degraded. The observed large V_{on} of 6.5 V and low current of 0.25 mA at 10 V suggest low conductivity, likely due to the rough fabric-like surface of high-M_n SPFN, as demonstrated by cAFM measurement in Figure 2c. Therefore, to enhance both optical and electrical performance, the utilization of MoO_x (<30 nm) and low-Mn SPFN (<50 kDa) with a smoother surface is recommended.

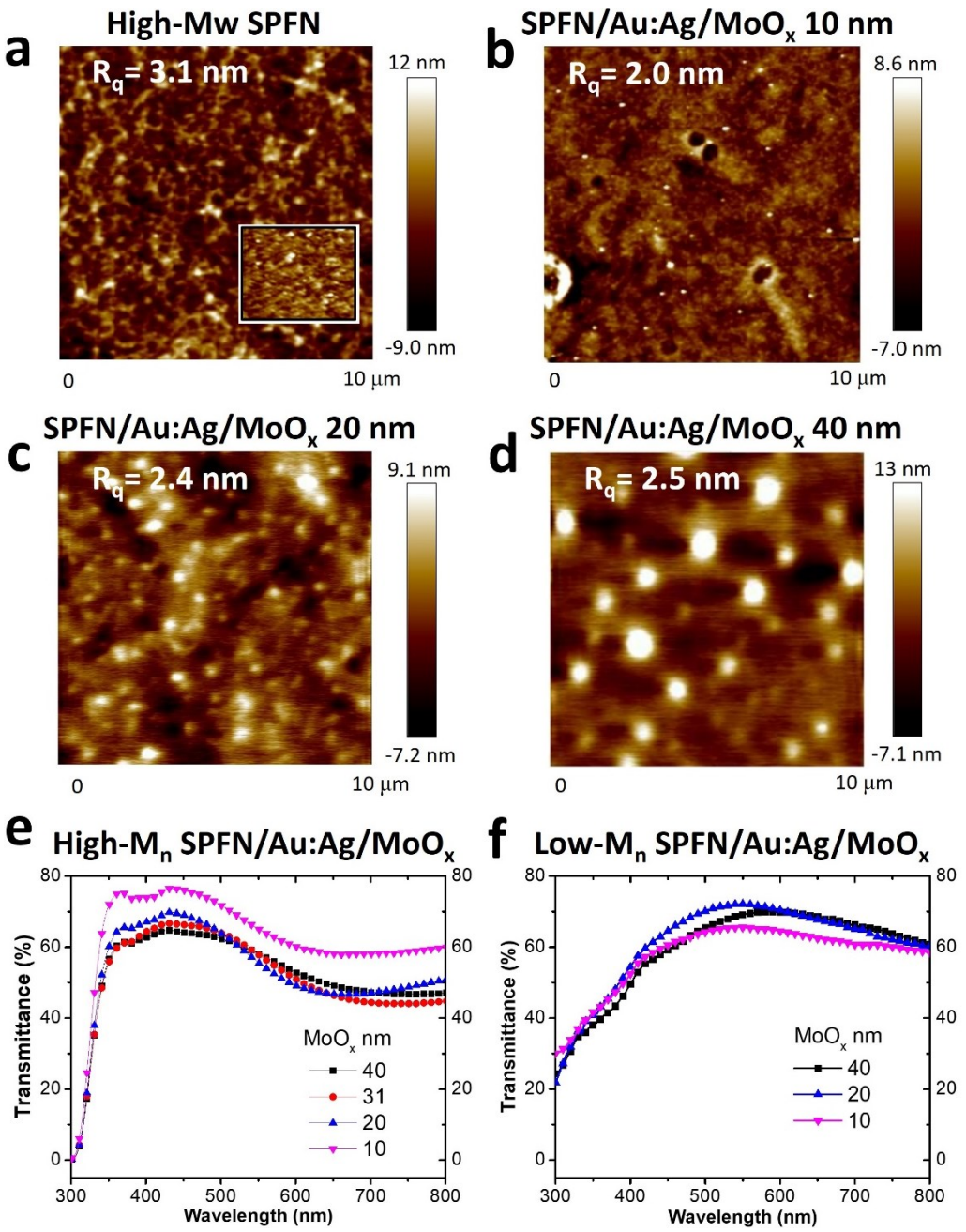

Figure S3. The topographies and roughness of the high-M_n SPFN (a) and 10 nm (b), 20 nm (c), and 40 nm (d) MoO_x on top of the hybrid drains. The inset in (a) is the topography of low-M_n SPFN with the roughness R_q=0.7 nm. Transmittance spectra of the hybrid drains composed of (e) high-M_n SPFN and (f) Low-M_n SPFN with different MoO_x thicknesses on top.

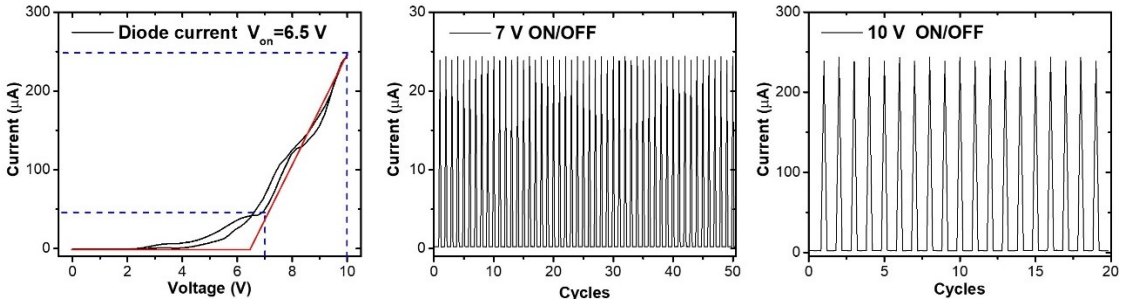

Figure S4. The I-V curve and the reliability tests on 7 V and 10 V of a functional diode composed of PATBT/SY/SPFN/Au:Ag/MoO_x multilayers.

S2. The measurements of Kelvin probe force microscope and conductive AFM on the hybrid drains:

The spun SPFN needs to be solvent-flushed to smoothen the surface and reduce the SPFN thickness to 2 nm for the Kelvin-probe and conductive AFM characterizations. Before flushing SPFN surface by methanol, the AFM tip frequently hit the aggregates on the SPFN surface shown in Figure S5 (Left) and produced jittering line profiles shown in Figure S5 (Right). After SPFN was flushed by methanol and was baked at 70 ℃ for 10 mins, the jittering lines can be removed. The topographic image and its corresponding surface potential mapping of SPFN were improved as shown in Figure 2b and their insets. Therefore, a smooth SPFN surface is required for the measurement of surface potential mapping and the following electrical operations.

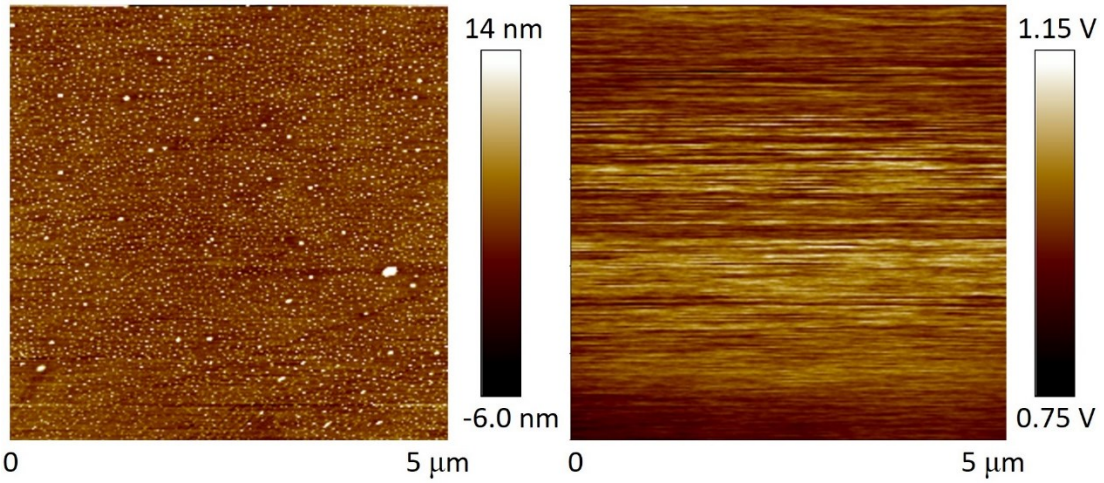

Figure S5 Left: The as-spun SPFN without methanol flushing. Right: The surface potential mapping.

ITO/PEDOT/SY and ITO/PEDOT/SY/SPFN were prepared for the electronic characterizations on the injection interface. Au-coated AFM tips were particularly chosen to better match the configuration of hybrid contacts (SPFN/Au/Ag). A conductive AFM was then applied to measure the morphology-dependent current in Figure 2c. After scanning from 0 to 10 V shown in Figure S6, the current values of SY with and without SPFN reveals a dramatic current enhancement by SPFN. The right-axis is a square root of current and can be depicted by space charge limited current

(SCLC), $I = J \cdot A = \frac{9}{8}\epsilon\mu A\frac{V^2}{d^3}$; ϵ, μ, V, and d are dielectric constant, carrier mobility, driving voltage, and the thickness of SY. The radius of Au-coated AFM tips is 15 nm. Fitting $\sqrt{I} - V$ curves of SY and SY/SPFN comes out two equations as following,

$$y_{SY} = 0.1718x - 0.4357 \text{ and } y_{SY/SPFN} = 0.8189x - 1.0712$$

The 1st slope 0.1718 of y_{SY} at low voltage regimes can obtain a mobility value 1.27×10^{-5} cm^2/Vs for SY while the slope 0.8189 of $y_{SY/SPFN}$ produces the mobility 2.89×10^{-4} cm^2/Vs. Figure S6 demonstrates the hybrid contacts can improve electron injection and significantly improve current conduction by 10-fold.

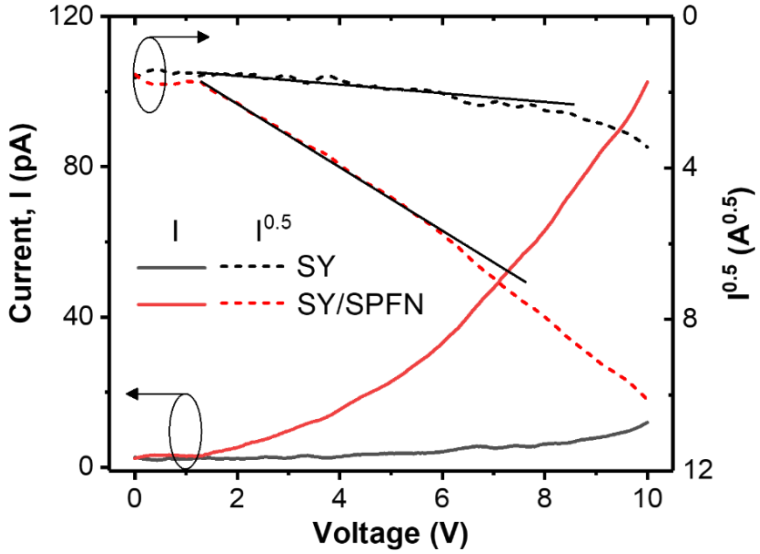

Figure S6 the I-V characteristics of SY and SY/SPFN obtained by a conductive AFM. The solid lines are the current of SY (black) and SY/SPFN (red). The dashed lines are the square root of currents.

S3. The correlation between mobility, EQE, and capture rate:

From Figure 4d, the averaged EQE in the two devices dropped, EQE_2/EQE_1=0.51%/0.23% is 2.29 closed to the mobility ratio of the two HC-OLEFETs 2.26 (μ_1/μ_2=0.52/0.23 extracted by the transconductance equation and Figure 4ab). The two nearly identical factors imply the direct correlation between EQE and hole fluxes. EQE can be read as following,

$$EQE = \eta_{out} \cdot \eta_{spin} \cdot \eta_{PL} \cdot \eta_c \quad \text{(S1)}$$

where η_{spin} is the singlet-to-triplet spin ratio, η_{PL} is the photoluminescent quantum yield, and η_{out} is the output coupling efficiency. We calculated the average capture efficiencies η_c for the two HC-OLEFETs with typical values of η_{spin}=0.25, η_{PL}=0.60 and η_{out}=0.20 and obtained η_c=0.17 for 0.23 cm^2/Vs and η_{cap}=0.067 for 0.52 cm^2/Vs. The ratio of two η_{cap} values is 2.21, similar to the mobility ratio 2.26.

In both transfer and output I-V curves (Figure 3ab), we can see HC-OLEFETs solely conducting holes. The small off-current ($\lesssim$30 nA) with sharp on/off ratio ($> 2 \times 10^4$) were almost identical to those of OTFTs composed of only PATBT[1]. The

similar p-type transport behaviors in HC-OLEFETs and OTFTs imply that there is no recombination current in both bilayer and monolayer transistor channels. In addition to the electrical properties, the EL of SY in Figure S2b have no luminescent features of PATBT[2] at 650 nm and 700 nm. Thus, both electrical and optical measurements showed no signs of electrons in PATBT. We concluded that the injected electrons were fully consumed in SY and did not interfered with the bottom p-type transistors. Hence, in Figure 4, electron density n and the recombination probability β are the two parameters to determine the EQE of the SY in the two devices (Note that hole density p is nearly identical in the operating devices determined by V_{GS} so $p(V_{GS})$ is chosen as a fitting variable in Section S4).

S4. The modeling procedures and the applied parameters:

For μ=0.23 and 0.52 $cm^2V^{-1}s^{-1}$, η_c=1/6 and 1/15 can be obtained using the equation S1 (Eqn. S1). By substituting η_c=1/6 and 1/15 into Eqn.1, an extreme mobility ratio $\mu_n/\mu_p \to 0$ can produce the max ratio of J_c/J_p 1/7 and 1/16 which match the averaged EQE values in Figure 4d.

$$\frac{J_c}{J_p} \sim \frac{J_n}{J_p} = \frac{n\mu_n}{p\mu_p} = \frac{1}{7} \text{ and } \frac{1}{16}; \text{ when totally recombined} \qquad \text{(S2)}$$

where contact width W=0.1 cm, length L=40 μm, SY thickness d=100 nm, C=10.7 nF/cm^2, $|V_{DS}|$ =100 V, μ= 0.23, and 0.52 cm^2/Vs. The maximum hole density in SY, p_{max} is assumed to have the same number of holes injected from the FET channel at $|V_{GS}|$ and is redistributed in the volume of the $0.1 \times 0.0012 \times 10^{-5}$ cm^3 below the hybrid drain, about 1.11×10^{16} cm^{-3} at $|V_{DS}|=|V_{GS}|$=100 V. The maximum electron density, n_{max}, is calculated by substituting J_c/J_p=1/7 and 1/16 into η_c to obtain Eqn. S2 at the extreme condition $\mu_n/\mu_p = 0$. Note that these calculated n and p values are only the preliminary fitting parameters and they only serve to properly initialize the simulation code. All the fitted n and β for different μ_n/μ_p values will be further optimized by the least-squares method in fitting.

S5. The relation between rubbing and transistor performance:

Groove density is an important parameter for transistor performance. Figure S7a shows the transconductance of PATBT transistors on the substrates rubbed 2, 4, 6, or 8 times using the procedure in the supporting information.[1] The rubbed nanostructures can change the dielectric strength. For the well-rubbed devices, the gate leakage current can be constrained within 4 nA as seen in Figure S7a. Leakage current was found to depend on the quality of lapping films. The SEM inspection in Figure S8 shows that there exist large diamond particles with sizes 0.9 to 2.0 μm in an unqualified lapping film while the most particles in the qualified one are more consistent with the 200 nm specification.

When large diamond particles create deep nanogrooves, gate leakage current will increase significantly as Figure S7b shows. We suggest using thick dielectrics >300 nm. Moreover, vender sides do exist quality variation in the purchased lapping films. It is important to monitor leakage current in a long term for the quality control in fabrication.

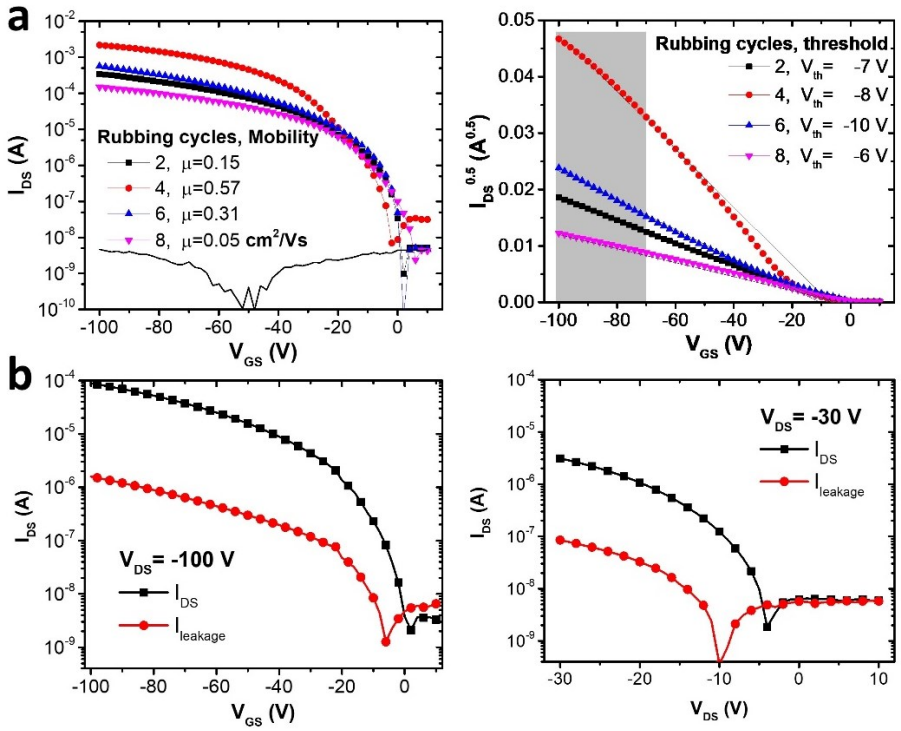

Figure S7. (a) The transconductance of the PATBT transistors on the substrates rubbed by diamond lapping film 2, 4, 6, and 8 cycles to produce different mobilities. The leakage current of the well-rubbed devices is about 4 nA. Threshold voltages vary between -6 to -10 V and the gray area is the saturation regime to extract the mobility values. (b) Voltage-dependent leakage current shows if using low-quality lapping films.

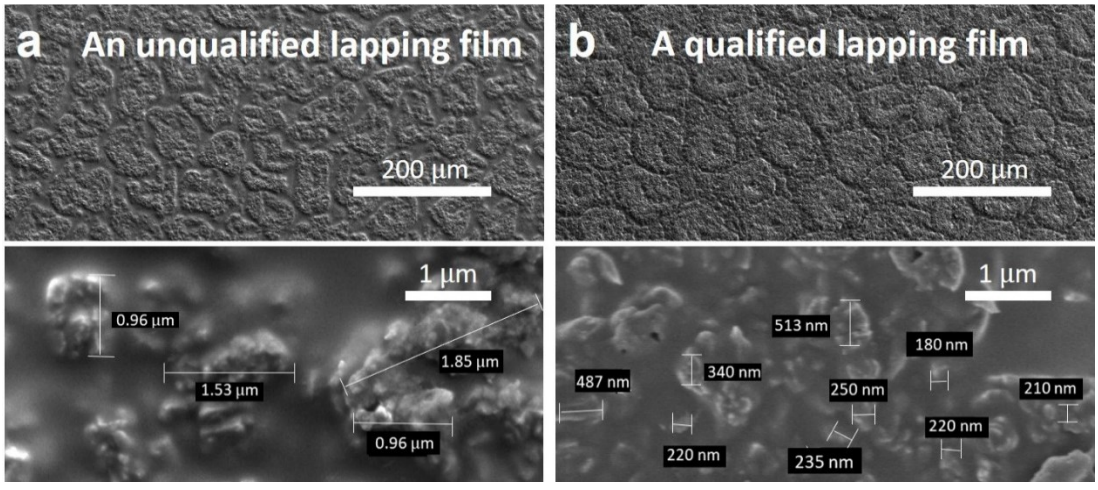

Figure S8. The SEM images of an unqualified lapping film (a) and a qualified one (b).

S6. The asymmetric source-drain contacts:

As the source and drain consist of different metals, they were deposited in the separate steps using two individual silicon shadow masks with source and drain patterns in Figure S9ab, respectively. Evaporated metal will go through the black areas and form electrodes. After combining two patterns by the alignment structures in depositions, the complete transistors were shown in Figure S9c and Figure 1a.

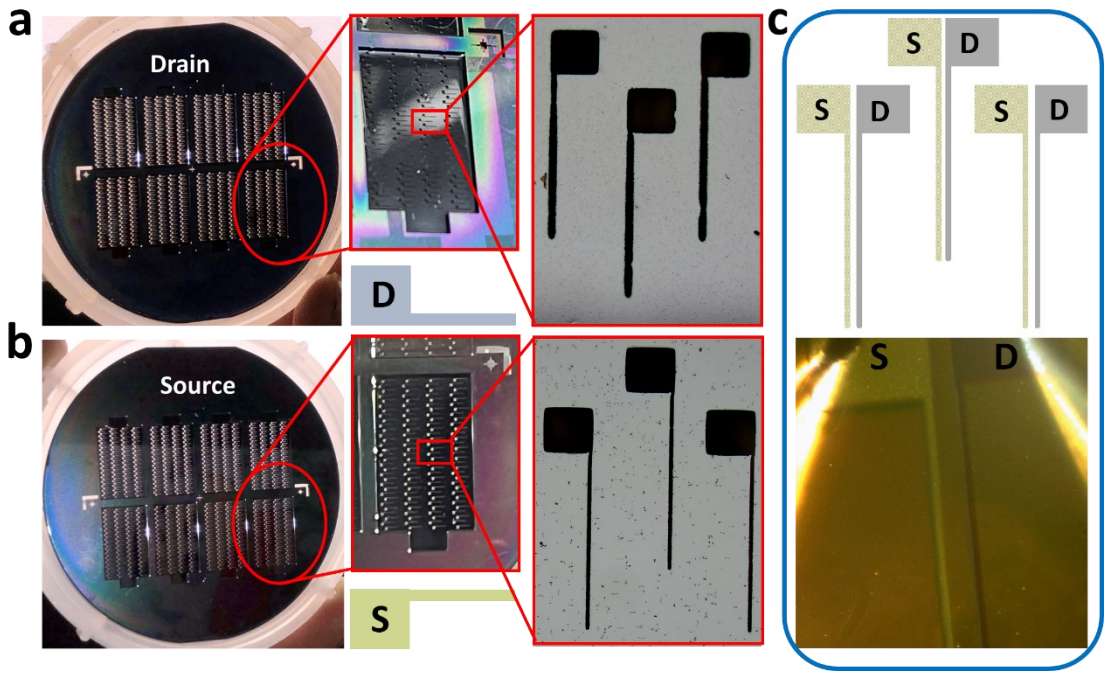

Figure S9. The designs of the two silicon shadow masks for drain **(a)**, source **(b)**, and alignment structures. **(c)** The combined patterns of source and drain electrodes and the images of the fabricated devices.

S7. The transfer and output discrepancy:

The phenomenon of "transfer I_{DS}> output I_{DS}" is commonly observed in low-mobility transistors made of amorphous or semicrystalline semiconductors. To evaluate the potential impact of this behavior, we analyzed organic transistors with commonly-seen channel lengths of 50 to 100 μm, operation voltages of 50 to 100 V, and mobilities $\mu=10^{-3}$ to 10 cm^2/Vs. Based on these parameters, we estimated the transit time $t_{tr} = L^2/V\mu = 2.0$ ms to 25 ns, indicating that larger t_{tr} values can reach the typical response times recorded in semiconductor parameter analyzers (5 to 20 ms). Therefore, transfer and output operations may result in different dynamic responses in organic transistors. Notably, we found that the I_{DS} difference between transfer and output is less severe or non-existent in $\mu \gtrsim 10$ cm^2/Vs.

The estimated t_{tr} in the millisecond scale suggests that the spatial charge effect can significantly impact channel conduction. When accelerating charges move through a fully charged channel at a large, constant V_{GS} in output operation, it takes longer to reach the highest conduction state at the scanning V_{DS}. However, during transfer operation at the highest constant V_{DS}, the entire channel can more quickly respond to the scanning V_{GS} and reach its highest conduction state. This discrepancy disappears when the transistor's mobility reaches about or exceeds 10 cm^2/Vs due to rapid charge transport. These findings are consistent with previous studies on high-mobility transistors composed of semiconducting small molecules,[3] polymers,[4] and metal oxides.[5]

S8. The ionic conjugated polyelectrolyte:

We investigated the use of an ionic conjugated polyelectrolyte, $PFN^+BIm_4^-$, as a replacement for the n-type SPFN in order to compare the EQE at various I_{DS}. By utilizing a concentration 0.05 wt% identical to that of SPFN in this work, we observed that the capture dynamics at increasing hole current fails to sustain the EQE value.

Instead, the EQE increases with hole current before decreasing rapidly at high I_{DS} regime, indicating a different capture mechanism. Previous works about OLEFETs[6-7] typically varied $PFN^{+}BIm_4^{-}$ concentration between 0.02 to 0.5 wt%, showing the highest performance at 0.02 wt%. We then attribute the low EQE here to the thick ionic CPE layer with degraded electron conductivity. Furthermore, the performance degradation observed with high molecular-weight SPFN in Figure S4 suggests possible issues with molecular weight that could contribute to the low EQE value in Figure S10.

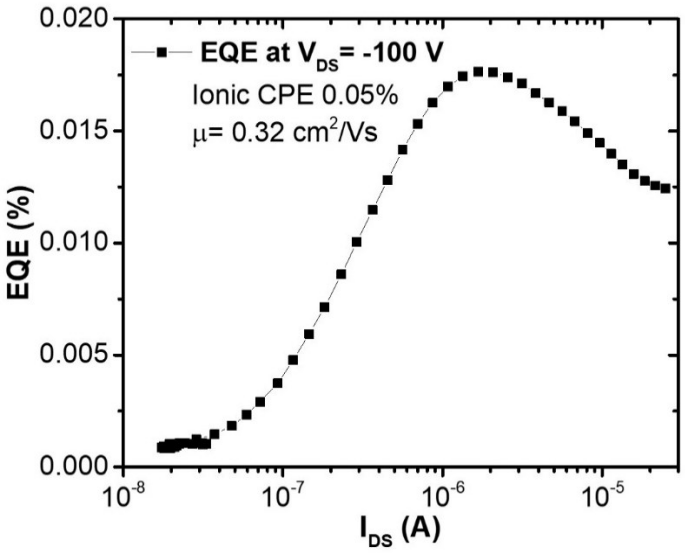

Figure S10. The EQE at various I_{DS} obtained from 0.05 wt% ionic CPE, $PFN^{+}BIm_4^{-}$ shows a different capture mechanism compared to n-type SPFN.

Reference:

1. Ordered Polymer Nanofibers Enhance Output Brightness in Bilayer Light-Emitting Field-Effect Transistors. *ACS Nano* **2013**, *7* (3), 2344–2351.

2. Photoinduced Charge Carrier Generation in Blends of Poly(Thienothiophene) Derivatives and [6,6]-Phenyl-C61-Butyric Acid Methyl Ester: Phase Segregation versus Intercalation. *J. Phys. Chem. C* **2010**, *114* (35), 15116–15120.

3. Ultra-high mobility transparent organic thin film transistors grown by an off-centre spin-coating method, *Nature Comm.* **2015**, 5:3005.

4. A Thienoisoindigo-Naphthalene Polymer with Ultrahigh Mobility of 14.4 cm^2/Vs that Substantially Exceeds Benchmark Values for Amorphous Silicon Semiconductors, *JACS* **2014**,136, 9477-9483.

5. Improved Performance of InGaZnO Thin-Film Transistor with HfLaO Gate Dielectric Annealed in Oxygen, *IEEE Trans. Device Mater. Reliab.* **2014**, 14, 177-181

6. Conjugated polyelectrolytes for organic light emitting transistors, *Appl. Phys. Lett.* **2010**, 97, 043303.

7. Solution-Processed Organic Light-Emitting Transistors Incorporating Conjugated

Polyelectrolytes, *Adv. Funct. Mater.* **2011**, 21, 3667-3672.